# NAPL Pool Dissolution in Stratified and Anisotropic Porous Formations

By Kenneth Y. Lee,[1] Student Member, ASCE, and Constantinos V. Chrysikopoulos[2]

**Abstract:** A two-dimensional numerical model is developed to study contaminant transport resulting from the dissolution of single- and multicomponent dense nonaqueous-phase liquid (DNAPL) pools in heterogeneous porous media. The aqueous-phase concentration of each dissolved component is assumed to undergo first-order decay as well as sorb under local equilibrium conditions. Pool shrinkage is accounted for by modeling the progressive reduction of the DNAPL pool surface area as a time-dependent boundary. Multicomponent pool dissolution is modeled using an effective solubility (or equilibrium aqueous solubility) relationship, where the nonaqueous-phase activity coefficient for each constituent is evaluated at each and every time step. Subsurface heterogeneities are depicted by an ideally stratified porous formation and by a statistically anisotropic aquifer. In the stratified formation, a multicomponent DNAPL pool is assumed to be formed at the interface between a sand layer and a clay layer, where DNAPL dissolution occurs simultaneously in both strata. The ground-water velocity inside the sand stratum is uniform in the longitudinal direction whereas the interstitial liquid in the aquitard is stagnant. In the statistically anisotropic aquifer, a single-component DNAPL pool is assumed to be formed on top of an impermeable bedrock, where DNAPL dissolution occurs in the aquifer only. Results from several model simulations indicate that dissolved contaminant concentrations in aquifers are reduced significantly in the presence of aquitards, and most importantly, the transfer of dissolved contaminants along the pool-water interface is slower within statistically anisotropic than within homogeneous aquifers.

## INTRODUCTION

The transport of contaminants resulting from the dissolution of nonaqueous-phase liquid (NAPL) pools recently has received considerable attention (e.g., Anderson et al. 1992; Johnson and Pankow 1992; Chrysikopoulos et al. 1994; Seagren et al. 1994; Voudrias and Yeh 1994; Whelan et al. 1994; Chrysikopoulos 1995; Lee and Chrysikopoulos 1995; Holman and Javandel 1996; Manivannan et al. 1996; Mason and Kueper 1996; Chrysikopoulos and Lee 1998). However, the majority of the NAPL dissolution studies published in the literature are associated with homogeneous porous media and do not examine the heterogeneous nature of complex natural subsurface formations.

Aquifers are often polluted with NAPL mixtures composed of two or more contaminants (Mackay et al. 1985; Mercer et al. 1990). The modeling of multicomponent NAPL dissolution involves the use of an effective solubility (or equilibrium aqueous solubility) relationship for each individual component. The effective solubility of each component in an NAPL mixture is equal to the single-component aqueous saturation concentration multiplied by the mole fraction of the component and its nonaqueous activity coefficient (Banerjee 1984). The nonaqueous-phase activity coefficient is a dimensionless parameter representing the component's degree of nonideality in the mixture (Stumm and Morgan 1981; Schwarzenbach et al. 1993), and it can be estimated by using the numerical code UNIFAC (UNI-functional group activity coefficients) created by Fredenslund et al. (1977).

In this work, a two-dimensional finite-difference multicomponent numerical model is developed to simulate solute transport resulting from the dissolution of well-defined, finite dense NAPL (DNAPL) pools in heterogeneous porous media. As the NAPL pool dissolves into the interstitial liquid of the aquifer or aquitard, a concentration boundary layer for each component is assumed to develop above or below the NAPL-water interface. The greater the concentration gradient the greater the mass transfer of the dissolved component. Therefore, it is assumed that the transfer of dissolved contaminants to the interstitial liquid is faster at the upstream compared with the downstream section of the DNAPL-water interface, which in turn leads to pool shrinkage and shifting of the pool origin in the downstream direction. Model simulations are performed for the longitudinal-vertical plane along the centerline of the pool. First, we considered a synthetic two-component DNAPL pool formed at the interface between a simple two-layered stratified formation consisting of a sand layer over a clay layer (Fig. 1). The pool is assumed to consist of a mixture of tetrachloroethylene (PCE) and 1,1,2-trichloroethane (1,1,2-TCA) because these compounds have dissimilar structures and form a nonideal DNAPL mixture. Each stratum (layer) is continuous with uniform hydraulic properties. This subsurface configuration permits NAPL dissolution into both strata simultaneously. Because ground-water flow rates in sand aquifers are orders of magnitude higher than in clay aquitards, the transport of dissolved contaminants is dominated by advective processes in the aquifer and diffusive processes in the aquitard. Furthermore, we considered a single-component 1,1,2-TCA pool formed on top of an impermeable bedrock in a statistically anisotropic aquifer, where NAPL dissolution is assumed to oc-

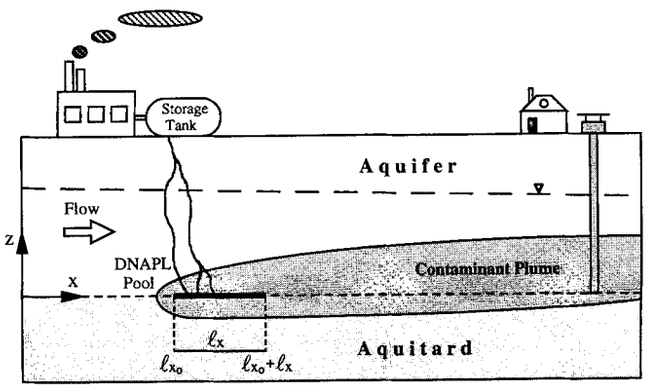


**FIG. 1. Schematic Representation of *xz* Cross Section along Centerline of DNAPL Pool of Length $l_x$ Showing Location of Pool with Respect to Origin of Cartesian Coordinate System**

[1]Grad. Student, Dept. of Civ. and Envir. Engrg., Univ. of California, Irvine, CA 92697.

[2]Assoc. Prof., Dept. of Civ. and Envir. Engrg., Univ. of California, Irvine, CA. To whom correspondence should be addressed.

Note. Editor: Byung R. Kim. Discussion open until February 1, 1999. To extend the closing date one month, a written request must be filed with the ASCE Manager of Journals. The manuscript for this paper was submitted for review and possible publication on September 9, 1997. This paper is part of the ***Journal of Environmental Engineering***, Vol. 124, No. 9, September, 1998. ©ASCE, ISSN 0733-9372/98/0009-0000–0000/ $8.00 + $.50 per page. Paper No. 16572.

cur in the aquifer only. The numerical model is good for verification of laboratory experiments as well as for cases where the subsurface pollution source can be represented by an idealized DNAPL pool.

## MODEL DEVELOPMENT

### Contaminant Transport

The governing partial differential equation describing the transient transport of each dissolved component originating from the dissolution of a DNAPL pool in saturated two-dimensional porous media, assuming that each component may sorb onto the solid matrix under local equilibrium conditions is

$$R_p \frac{\partial C_p(t, x, z)}{\partial t} = \frac{\partial}{\partial x}\left[D_{x_p}(x, z)\frac{\partial C_p(t, x, z)}{\partial x}\right] + \frac{\partial}{\partial z}\left[D_{z_p}(x, z)\frac{\partial C_p(t, x, z)}{\partial z}\right] - \frac{\partial}{\partial x}[U_x(x, z)C_p(t, x, z)] - \frac{\partial}{\partial z}[U_z(x, z)C_p(t, x, z)] - \lambda_p R_p C_p(t, x, z) \quad (1)$$

where $C$ = aqueous-phase solute concentration; $D_x$ and $D_z$ = longitudinal and vertical hydrodynamic dispersion coefficients, respectively; $R$ = dimensionless retardation factor; $U_x$ and $U_z$ = interstitial fluid velocities in the longitudinal and vertical directions, respectively; $t$ = time; $x$ and $z$ = spatial coordinates in the longitudinal and vertical directions, respectively; $\lambda$ = first-order decay constant; and subscript $p$ = component indicator. It should be noted that the term $\lambda RC$ in (1) implies that the decay coefficient of the aqueous-phase concentration is identical to the decay coefficient of the concentration sorbed onto the solid matrix. The governing partial differential equation (1) is linear with respect to the aqueous-phase concentration; however, a closed-form analytical solution cannot be obtained because $D_x$, $D_z$, $U_x$, and $U_z$ are functions of the spatial coordinates. Thus, a numerical approximation was developed.

For a well-defined multicomponent DNAPL pool with finite mass and uniform thickness formed at the interface between two stratified formations (i.e., aquifer/aquitard, Fig. 1), the transfer of each component from the NAPL-water interfaces to the interstitial fluid in both aquifer and aquitard is described by the following mass transfer relationships (Chrysikopoulos et al. 1994):

$$-\mathcal{D}_{e_p}\frac{\partial C_p(t, x, 0^+)}{\partial z} = k_p(t, x)[C_p^w(t) - C_p(t, x, +\infty)], \quad l_{x_0} < x < l_{x_0} + l_x \quad (2)$$

$$\hat{\mathcal{D}}_{e_p}\frac{\partial C_p(t, x, 0^-)}{\partial z} = \hat{k}_p(t, x)[C_p^w(t) - C_p(t, x, -\infty)], \quad l_{x_0} < x < l_{x_0} + l_x \quad (3)$$

where $\mathcal{D}_{e_p} = \mathcal{D}_p/\tau^*$ = effective molecular diffusion coefficient of component $p$; $\mathcal{D}$ = molecular diffusion coefficient; $\tau^* \geq 1$ = tortuosity; $k(t, x)$ = local mass transfer coefficient applicable at the pool-water interface; the "hat" represents parameters associated with the aquitard; $l_{x_0}$ = location of the pool's origin; and $l_x$ = pool length (Fig. 1). The interface of the two strata is at $z = 0$ and superscripts "+" and "−" indicate locations slightly above or slightly below the aquifer/aquitard interface. It should be noted that (2) and (3) assumed that the thickness of the pool is insignificant relative to the thickness of the porous medium. Furthermore, $C^w$ is the time-dependent effective solubility calculated by using the following expression (Banerjee 1984; Lee and Chrysikopoulos 1995):

$$C_p^w(t) = C_{s_p} X_p(t)\gamma_p(X_p) \quad (4)$$

where $C_s$ = pure component saturation concentration (solubility); $X$ = time-dependent nonaqueous-phase mole fraction of component $p$; and $\gamma$ = mole fraction–dependent nonaqueous-phase activity coefficient of component $p$. For the special case where the NAPL mixture behaves ideally, $\gamma_p \simeq 1$, (4) reduces to Raoult's law. For a single-component NAPL the effective solubility is constant and equal to the aqueous saturation concentration $C^w(t) = C_s$. Also, it should be noted that $C_p(t, x, \pm\infty)$ is the bulk or background concentration of component $p$ in the interstitial fluid. Conventionally, any location outside

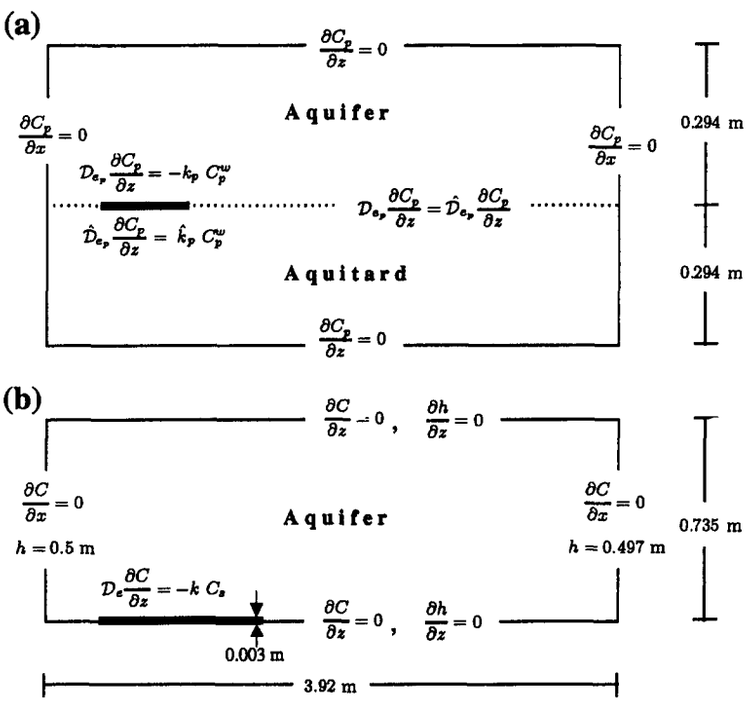


**FIG. 2. Schematic Illustration of Numerical Domain for: (a) Stratified Aquifer; (b) Statistically Anisotropic Aquifer**

the concentration boundary layer is considered as $z \rightarrow \pm\infty$ (Incropera and DeWitt 1990).

The appropriate initial and boundary conditions for the case of a multicomponent DNAPL pool formed at the interface between two stratified formations are

$$C_p(0, x, z) = 0 \tag{5}$$

$$C_p(t, \pm\infty, z) = 0 \tag{6}$$

$$\mathcal{D}_{e_p} \frac{\partial C_p(t, x, 0^+)}{\partial z} = -k_p(t, x) C_p^w(t) \quad l_{x_0} < x < l_{x_0} + l_x \tag{7}$$

$$\hat{\mathcal{D}}_{e_p} \frac{\partial C_p(t, x, 0^-)}{\partial z} = \hat{k}_p(t, x) C_p^w(t) \quad l_{x_0} < x < l_{x_0} + l_x \tag{8}$$

$$\mathcal{D}_{e_p} \frac{\partial C_p(t, x, 0^+)}{\partial z} = \hat{\mathcal{D}}_{e_p} \frac{\partial C_p(t, x, 0^-)}{\partial z} \quad x < l_{x_0}, x > l_{x_0} + l_x \tag{9}$$

$$C_p(t, x, \infty) = 0 \tag{10}$$

Eqs. (7) and (8) are identical to (2) and (3) with background concentration $C_p(t, x, \pm\infty) = 0$.

For the case of the statistically anisotropic aquifer, a single-component DNAPL pool is considered in this work. Therefore, the subscript $p$ can be removed from the governing equations, and (3), (4), (8), and (9) are no longer applicable because the pool is assumed to be formed on top of an impermeable bedrock.

## Ground-Water Flow

For the stratified formation case, the interstitial ground-water velocity within the aquifer is assumed to be unidirectional and invariant ($U_x$ = constant; $U_z = 0$). However, for the statistically anisotropic aquifer case, the velocity components in the $x$- and $z$-directions are spatially variable.

Statistically anisotropic, two-dimensional, log-transformed hydraulic conductivity fields are generated based on the following widely used exponentially decaying covariance function (Gelhar and Axness 1983; Sudicky 1986; Russo et al. 1994):

**TABLE 1. Parameter Values for Numerical Simulations**

| Parameter (1) | Stratified formation (2) | Statistically anisotropic aquifer (3) |
|---|---|---|
| $C_b$, $\hat{C}_b$ (g/L) | 0.0[a,b] | 0.0[b] |
| $C_s$ (g/L) | 0.15[a], 4.5[b] | 4.5[b] |
| $D_x$ (m²/h) | $1.01 \times 10^{-4}$[a,b] | Spatially variant |
| $D_z$ (m²/h) | $1.21 \times 10^{-5}$[a], $1.22 \times 10^{-5}$[b] | Spatially variant |
| $\mathcal{D}_e$ (m²/h) | $2.19 \times 10^{-6}$[a], $2.33 \times 10^{-6}$[b] | $2.33 \times 10^{-6}$[b] |
| $\hat{\mathcal{D}}_e$, $\hat{D}_x$, $\hat{D}_z$ (m²/h) | $3.13 \times 10^{-7}$[a], $3.33 \times 10^{-7}$[b] | — |
| $d$ (m) | 0.003 | 0.003 |
| $\mathcal{M}'$ (mol) | 0.74[a], 0.74[b] | — |
| $R$ | 2.89[a], 1.63[b] | 1.63[b] |
| $\hat{R}$ | 5.78[a], 3.26[b] | — |
| $U_x$ (m/h) | $3.0 \times 10^{-3}$ | Spatially variant |
| $U_z$ (m/h) | 0.0 | Spatially variant |
| $\hat{U}_x$, $\hat{U}_z$ (m/h) | 0.0 | — |
| $\hat{\gamma}$ | — | 0.8 |
| $\alpha_L$ (m) | $3.3 \times 10^{-2}$ | $3.3 \times 10^{-2}$ |
| $\alpha_T$ (m) | $3.3 \times 10^{-3}$ | $3.3 \times 10^{-3}$ |
| $\Delta t$ (h) | 5 | 5 |
| $\zeta_x$ (m) | — | 0.5 |
| $\zeta_z$ (m) | — | 0.06 |
| $\lambda$ ($h^{-1}$) | 0.0[a,b] | 0.0[b] |
| $\tau^*$ | 1.43 | 1.43 |
| $\hat{\tau}^*$ | 10.0 | — |
| $\theta$ | 0.3 | 0.3 |
| $\hat{\theta}$ | 0.05 | — |

[a]Data for PCE.
[b]Data for 1,1,2-TCA.

$$\text{Cov}(\mathbf{r}) = \sigma_Y^2 \exp\left[-\left(\frac{r_x^2}{\zeta_x^2} + \frac{r_z^2}{\zeta_z^2}\right)^{1/2}\right] \tag{11}$$

where $\sigma_Y^2$ = variance of the log-transformed hydraulic conductivity ($Y = \ln K$, where $K$ is the hydraulic conductivity); $\mathbf{r} = (r_x, r_z)^T$ = a two-dimensional vector whose magnitude is the separation distance of two hydraulic conductivity measurements; and $\zeta_x$ and $\zeta_z$ = longitudinal and vertical correlation length scales, respectively. It should be noted that statistical anisotropy implies that the covariance function depends on both the magnitude and the direction of the separation vector (Gelhar 1993). For each realization of the hydraulic conductivity field generated, a spatially variant head field can be determined numerically by the following two-dimensional equation, which describes steady-state flow through a heterogeneous, isotropic, saturated porous medium (Bear 1979):

$$\frac{\partial}{\partial x}\left[K(x, z)\frac{\partial h(x, z)}{\partial x}\right] + \frac{\partial}{\partial z}\left[K(x, z)\frac{\partial h(x, z)}{\partial z}\right] = 0 \tag{12}$$

where $h$ = total head potential. It should be noted that $K(x, z)$ is locally independent of direction and hydraulic anisotropy is

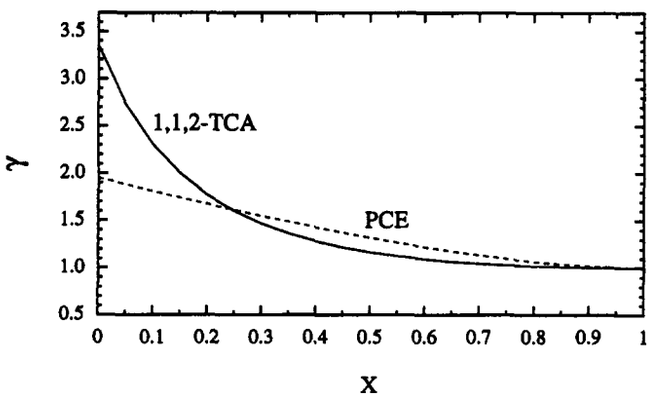


**FIG. 3. Nonaqueous-Phase Activity Coefficients as Function of Mole Fraction Estimated with UNIFAC for Mixture of PCE and 1,1,2-TCA**

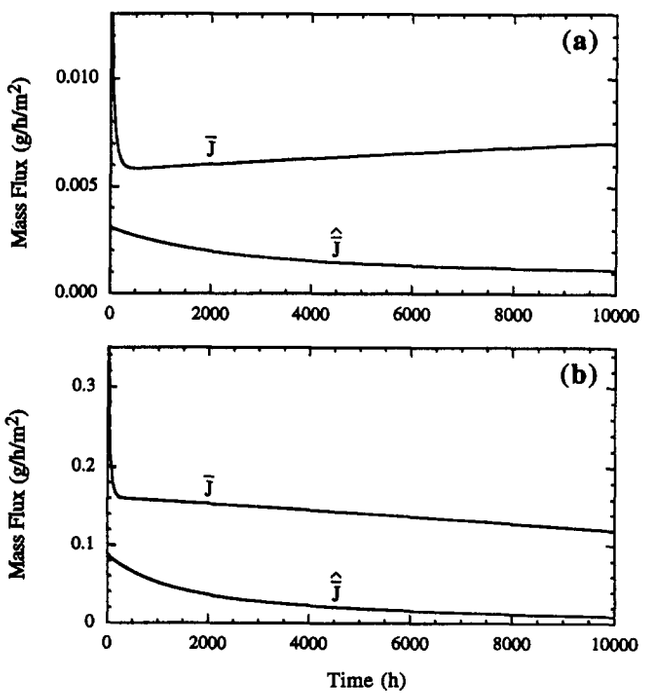


**FIG. 4. Calculated Average Mass Fluxes as Function of Time for: (a) PCE; (b) 1,1,2-TCA**

introduced by the overall spatial variability of the hydraulic conductivity field (Burr et al. 1994). Furthermore, the hydraulic conductivity is time invariant because the DNAPL pool is assumed to remain immobile (single-phase flow); thus, the porous formation is water saturated continuously. Velocity components in the $x$- and $z$-directions are then calculated for every discretized point (node) within the aquifer by using the following form of Darcy's equation:

$$U_x(x, z) = -\frac{K(x, z)}{\theta}\frac{\partial h(x, z)}{\partial x} \tag{13}$$

$$U_z(x, z) = -\frac{K(x, z)}{\theta}\frac{\partial h(x, z)}{\partial z} \tag{14}$$

where $\theta$ = effective porosity. In this study, it is assumed that the porosity maintains a constant value because the spatial variability of porosity is considered to be much smaller than the variability of hydraulic conductivity; thus, the variability of the porosity is not a factor that will significantly affect steady flow (Freeze 1975; Dagan 1989).

## Numerical Solution

The two-dimensional mathematical model presented is solved numerically by a fully implicit, finite-difference scheme. Discretization of the governing partial differential equation (1) results in a band diagonal system of equations. Each node contributes an equation. However, the number of equations to be considered is limited by the memory size of the available computer. In this study, a Sparc 20 workstation (Sun Microsystems) with 80 MB of physical random-access memory is used. This particular system is capable of efficiently solving a band diagonal matrix corresponding to approximately 2,500 equations.

The numerical domain as well as the corresponding boundary conditions for both cases of heterogeneous formations considered in this study are illustrated schematically in Fig. 2. For the stratified aquifer [Fig. 2(a)], the subsurface domain is divided into two subdomains, a top subdomain representing the aquifer and a bottom subdomain representing the aquitard. Splitting the subsurface into two subdomains results in two separate band diagonal matrices, and each matrix can be solved independently. The number of nodes used for each subdomain in the $x$- and $z$-directions are 50 and 50 with a nodal separation distance of 0.08 and 0.006 m, respectively. A no-dispersive flux condition is applied to all outer boundaries of the numerical domain. Eq. (7) is applied to the nodes at the pool-water interface within the aquifer subdomain, whereas (8) is applied to the nodes at the pool-water interface within the aquitard subdomain. The matrices are solved recursively at each and every time step, and (9) is satisfied by requiring the two subdomains to share the same nodal points at the aquifer/aquitard interface.

For the statistically anisotropic aquifer [Fig. 2(b)], only (7) is applied to the nodes at the pool-water interface within the aquifer domain. A no-dispersive flux condition also is applied to all outer boundaries of the numerical domain. The number of nodes used in the aquifer in the $x$- and $z$-directions are 50 and 50 with a nodal separation distance of 0.08 and 0.015 m,

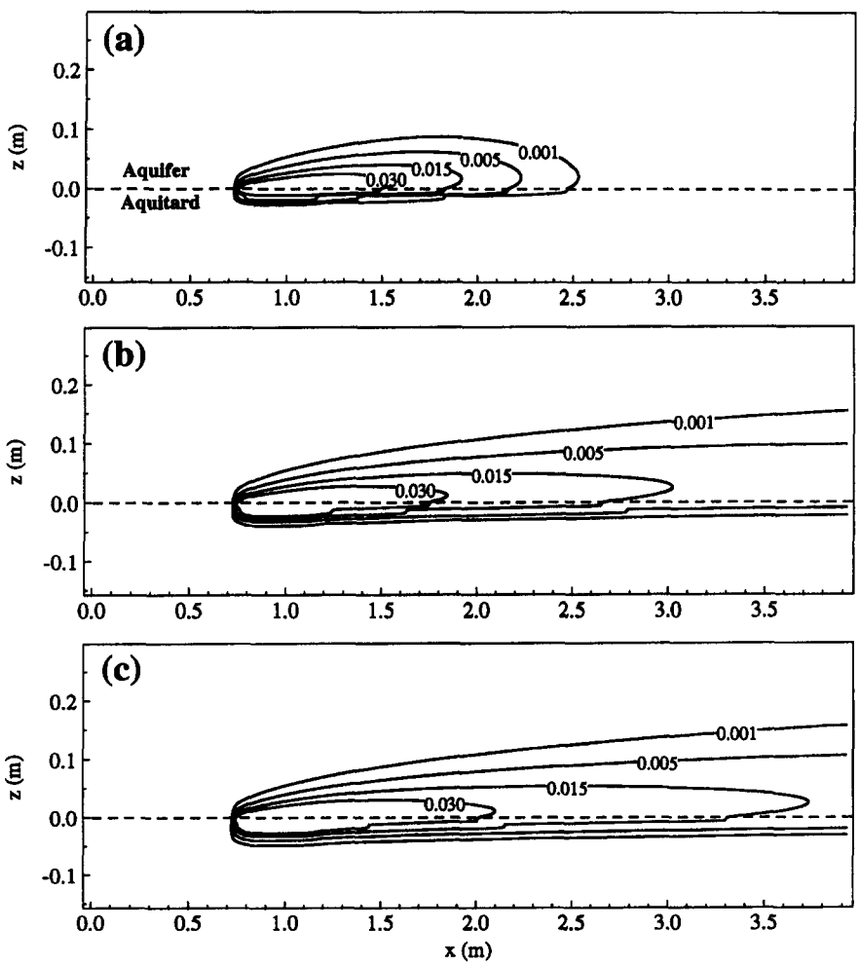


**FIG. 5. Concentration Contour Plots of PCE (g/L) in Stratified Formation Consisting of Sand Stratum over Clay Stratum at: (a) 1,000; (b) 5,000; (c) 10,000 h (after Initiation of Dissolution Process)**

respectively. The head field is obtained by discretizing the flow equation (12) in a similar fashion to the discretization of the transport equation (1). Constant head values are applied at the upstream and downstream numerical boundaries; furthermore, the top and bottom numerical boundaries are considered impervious.

## EVALUATION OF MODEL PARAMETERS

The aqueous-phase molecular diffusion coefficient for each constituent of the DNAPL pool is obtained by using the Hayduk and Laudie relationship (Hayduk and Laudie 1974)

$$\mathfrak{D}_p = \frac{4.77 \times 10^{-5}}{\eta_w^{1.14} V_p^{0.589}} \left[\frac{\text{m}^2}{\text{h}}\right] \tag{15}$$

where $\eta_w$ (cP) = viscosity of water [at 25°C $\eta_w$ = 0.8904 cP, Lyman et al. (1982)]; and $V$ ($\text{cm}^3$/mol) is the molar volume. The molar volume of each constituent is estimated using the LeBas method, which sums the volume increments of every individual atom in the molecule and subtracts any volume correction for the shape or structure of the molecule (Lyman et al. 1982). The LeBas molar volumes for PCE and 1,1,2-TCA are 128.0 and 115.0 $\text{cm}^3$/mol, respectively (Mackay et al. 1992). Employing a tortuosity of $\tau^* = 1.43$ for sand and $\hat{\tau}^* = 10.0$ for clay (de Marsily 1986), the calculated effective molecular diffusion coefficient for PCE is $2.19 \times 10^{-6}$ $\text{m}^2$/h in sand and $3.13 \times 10^{-7}$ $\text{m}^2$/h in clay; for 1,1,2-TCA, it is $2.33 \times 10^{-6}$ $\text{m}^2$/h in sand and $3.33 \times 10^{-7}$ $\text{m}^2$/h in clay.

The hydrodynamic dispersion coefficients are obtained by the following relationships (Bear 1979):

$$D_x(x, z) = \frac{\alpha_T U_z^2(x, z) + \alpha_L U_x^2(x, z)}{|\mathbf{U}|} + \mathfrak{D}_e \tag{16}$$

$$D_z(x, z) = \frac{\alpha_T U_x^2(x, z) + \alpha_L U_z^2(x, z)}{|\mathbf{U}|} + \mathfrak{D}_e \tag{17}$$

where

$$|\mathbf{U}| = [U_x^2(x, z) + U_z^2(x, z)]^{1/2} \tag{18}$$

is the magnitude of the interstitial velocity vector; and $\alpha_L$ and $\alpha_T$ = longitudinal and transverse dispersivities in the $x$- and $z$-directions, respectively.

For instantaneous, reversible sorption with a linear isotherm, the retardation factor in the aquifer is (Hashimoto et al. 1964)

$$R_p = 1 + \frac{\rho_b}{\theta} K_{d_p} \tag{19}$$

where $\rho_b$ = bulk density of the aquifer; and $K_d$ = distribution coefficient, which can be estimated using the correlation (Karickhoff 1984)

$$K_{d_p} = f_{oc} K_{oc_p} \tag{20}$$

where $f_{oc}$ = organic carbon fraction of the porous medium; and $K_{oc}$ = organic carbon partition coefficient (mass sorbed per unit mass of organic carbon per unit aqueous concentration). It should be noted that calculation of $K_d$ based on (20) is accurate when sorption can be represented by a linear model and occurs primarily onto organic carbon (Ball and Roberts 1991). The $K_{oc}$ values for PCE and 1,1,2-TCA used in this work are 2.1

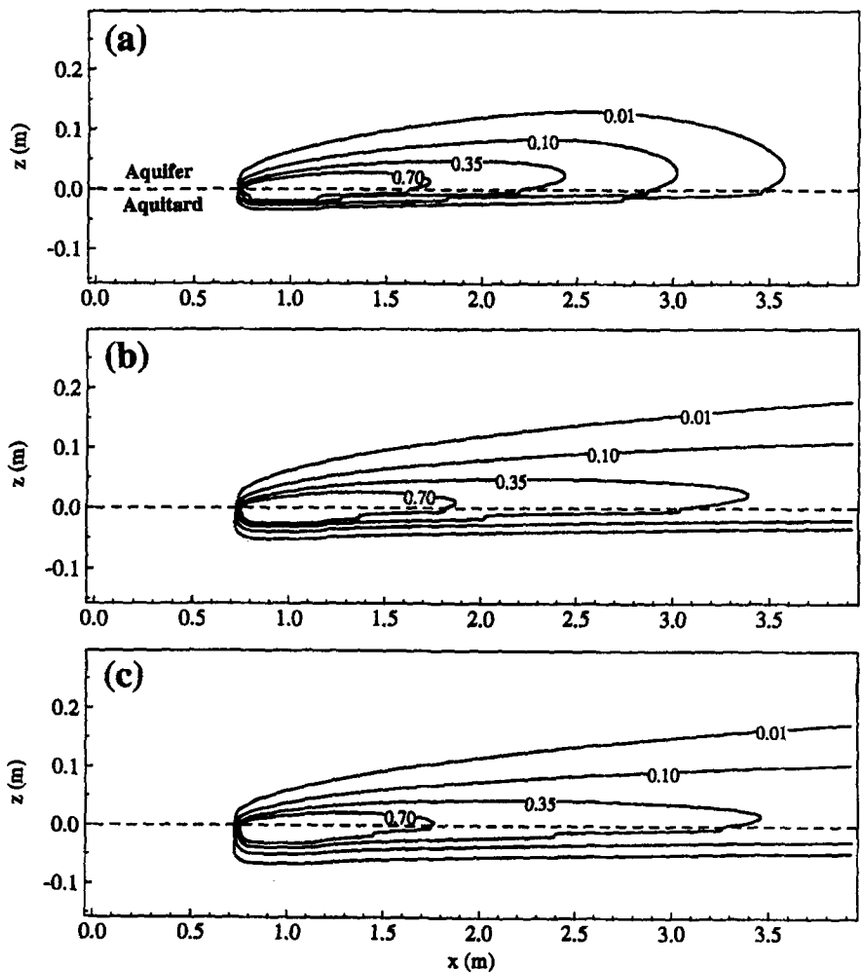


**FIG. 6. Concentration Contour Plots of 1,1,2-TCA (g/L) in Stratified Formation Consisting of Sand Stratum over Clay Stratum at: (a) 1,000; (b) 5,000; (c) 10,000 h (after Initiation of Dissolution Process)**

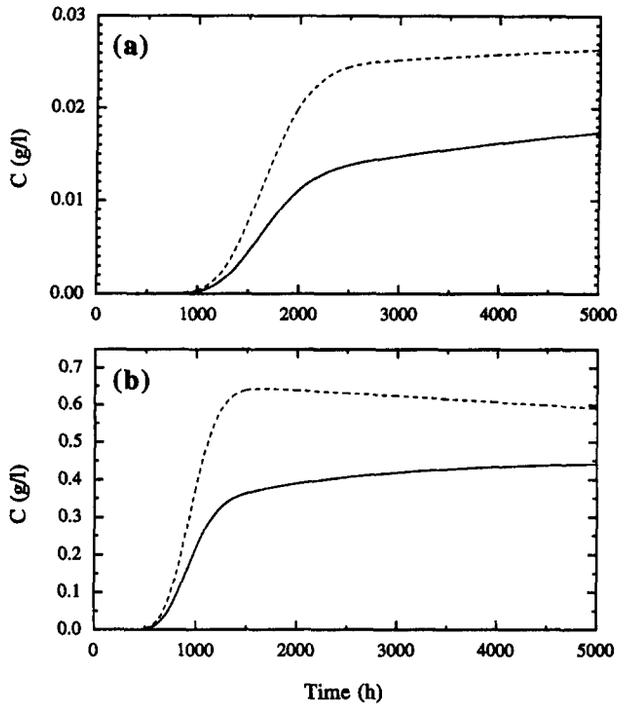


**FIG. 7. Comparison between Predicted Breakthrough Curves with (Solid Lines) and without (Dashed Lines) Contaminant Diffusion into Aquitard for: (a) PCE; (b) 1,1,2-TCA (Here $x = 2.72$ m; $z = 0.024$ m)**

$\times 10^{-4}$ and $7.0 \times 10^{-5}$ m$^3$/g, respectively (Mackay et al. 1992). Assuming the aquifer has a bulk density of $1.69 \times 10^6$ g/m$^3$, an effective porosity of 0.3, and an organic carbon fraction of $f_{oc} = 0.16\%$, the retardation factors for PCE and 1,1,2-TCA are estimated as 2.89 and 1.63, respectively. In clay-rich formations, contaminant sorption occurs onto both organic and inorganic solids (Karickhoff 1984; Myrand et al. 1992). Thus, $K_d$ calculations for clay-rich aquitards may not be accurate if based on (20). However, retardation factors reported in the literature for organic contaminants in clay formations are a few-fold higher than the corresponding retardation factors in other types of porous media. In this study, the retardation factor for each dissolved component is assumed to be twice as large in the aquitard as in the aquifer ($\hat{R}_p = 2R_p$). Table 1 summarizes the parameter values used in the simulations.

For each time step the multicomponent pool composition is updated, $X$ and $\gamma$ are evaluated accordingly, and $C^w$ is calculated for each component using (4). The nonaqueous-phase activity coefficients required for the evaluation of the time-dependent equilibrium aqueous solubilities are obtained with the software PC-UNIFAC (BRI 1993). The UNIFAC is a semi-empirical thermodynamic model developed by Fredenslund et al. (1977) to estimate activity coefficients of nonideal liquid mixtures.

The nonaqueous-phase mole fraction of each component $X_p(t)$ is calculated at each time step by dividing the number of moles of each component by the total number of moles present in the pool. The number of moles for each component as a function of time $\mathcal{M}_p(t)$ is calculated by tracking the amount of contaminant mass depleted from the pool during all preceding time steps using the following relationship:

$$\mathcal{M}_p(t) = \mathcal{M}'_p - \frac{[\theta \bar{k}_p(t) + \hat{\theta}\hat{\bar{k}}_p(t)]\Delta t}{(\text{mol wt})_p} \sum_{m=1}^{m_f} C_p^w(m\Delta t)A(m\Delta t) \quad t \geq \Delta t \tag{21}$$

where $\mathcal{M}'_p$ = initial number of moles of component $p$ in the nonaqueous phase; $\Delta t$ = time step; and $m$ = an integer time step summation index with $m_f = \mathrm{I}(t/\Delta t)$ indicating the total number of time steps, where I( ) is an integer mode arithmetic operator truncating any fractional part of the numeric argument; $\bar{k}(t)$ and $\hat{\bar{k}}(t)$ = time-dependent, spatially averaged (or overall) mass transfer coefficients for the aquifer and aquitard, respectively; and $A(t)$ = pool surface area. The time-dependent pool-water interfacial area is calculated using

$$A(t) = \sum_{p=1}^{\mathcal{P}} \frac{\mathcal{M}_p(t)(\text{mol wt})_p}{\rho_p \theta d} \tag{22}$$

where $d$ = thickness of the NAPL pool; $\mathcal{P}$ indicates the total number of components in the mixture; and $\rho_p$ = fluid density of component $p$. The fluid density and the molecular weight for PCE are $1.63 \times 10^6$ g/m$^3$ and 165.83 g/mol, respectively; and for 1,1,2-TCA, they are $1.44 \times 10^6$ g/m$^3$ and 133.41 g/mol, respectively (Mackay et al. 1992).

The DNAPL pool shrinkage caused by dissolution is accounted for at each time step of the numerical approximation. Chrysikopoulos (1995) noted that the longer the pool in the direction of flow, the higher the solute peak concentration in the interstitial fluid. Consequently, as the pool shrinks, the dissolved peak concentration decreases. Therefore, it is important to account for pool shrinkage. Assuming that the ratio of the pool length to pool width is equal to a time invariant parameter

$$\xi = \frac{l_x(t)}{l_y(t)} = \text{constant} \tag{23}$$

where $l_y$ = pool width, the time-dependent coordinate of the pool origin (Fig. 1), is given by

$$l_{x_0}(t) = l_{x_0}(t - \Delta t) + l_x(t - \Delta t) - [\xi A(t)]^{1/2} \tag{24}$$

The local mass fluxes $J$ and $\hat{J}$ along the length of the pool are calculated in this study at each time step using (7) and (8) as follows:

$$J_p(t, x) = C_p^w(t)k_p(t, x) = -\mathcal{D}_{e_p}\frac{\partial C_p(t, x, 0^+)}{\partial z} \quad l_{x_0} < x < l_{x_0} + l_x \tag{25}$$

$$\hat{J}_p(t, x) = C_p^w(t)\hat{k}_p(t, x) = \hat{\mathcal{D}}_{e_p}\frac{\partial C_p(t, x, 0^-)}{\partial z} \quad l_{x_0} < x < l_{x_0} + l_x \tag{26}$$

where the derivatives of concentration with respect to $z$ are obtained by numerically solving the governing partial differential in (1) in conjunction with the following boundary conditions:

$$C_p(t, x, 0^+) = C_p^w(t) \quad l_{x_0} < x < l_{x_0} + l_x \tag{27}$$

$$C_p(t, x, 0^-) = C_p^w(t) \quad l_{x_0} < x < l_{x_0} + l_x \tag{28}$$

which imply that the concentration along each pool-water interface within the porous formation is equal to the effective solubility of the corresponding component. The average mass transfer coefficients $\bar{k}(t)$ and $\hat{\bar{k}}(t)$ at each time step are calculated by averaging the calculated local mass transfer coefficients over the corresponding pool-water interfacial area. Furthermore, the average mass fluxes $\bar{J}(t)$ and $\hat{\bar{J}}(t)$ are calculated by using the relationships $\bar{J}(t) = C^w(t)\bar{k}(t)$ and $\hat{\bar{J}}(t) = C^w(t)\hat{\bar{k}}(t)$, respectively. It should be noted that the calculation of $\mathcal{M}_p(t)$ is based on average mass transfer coefficients applied to the entire surface of the pool [see (21)]. For the case of a single-component DNAPL pool formed within a statistically anisotropic aquifer, the average mass flux is obtained in a similar fashion; however, the subscript $p$ is removed from the governing equations (1), (25), and (27); the effective solubility is replaced by $C_s$; and (26) and (28) are no longer applicable.

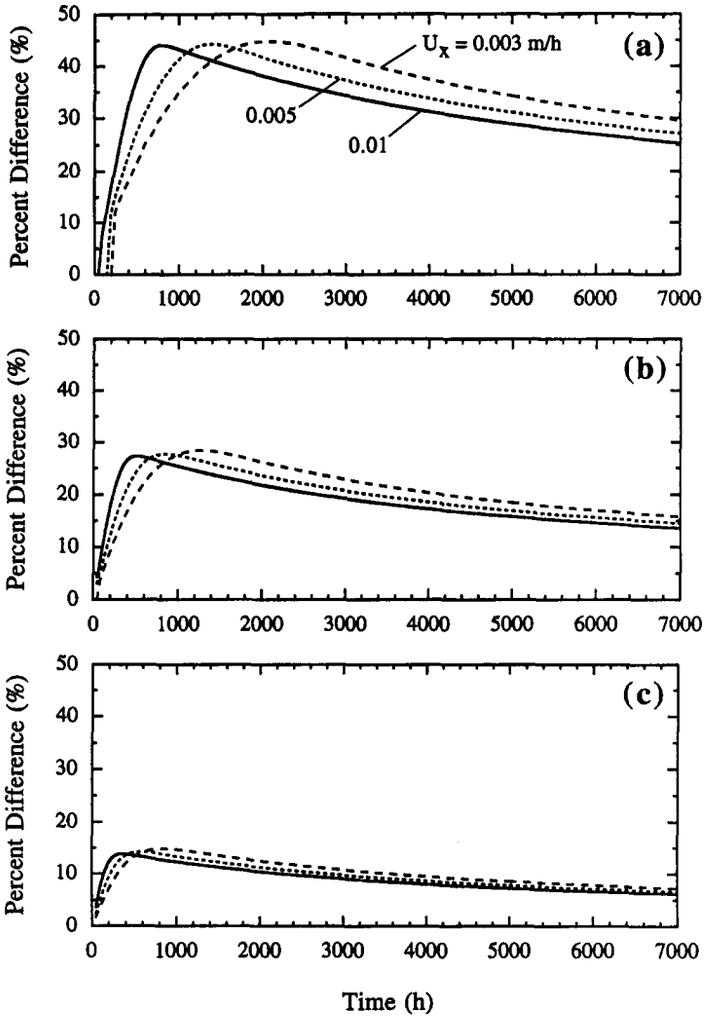


**FIG. 8. Comparison of Dissolved Concentrations Originating from Single-Component PCE Pool with and without Diffusion into Aquitard as Function of Time for Three Ground-Water Velocities at Downstream Locations: (a) $x = 2.72$ m; (b) $x = 1.92$ m; (c) $x = 1.52$ m (Here $\hat{R} = 5.78$; $z = 0.024$ m)**

## SIMULATIONS AND ANALYSIS

### Ideally Stratified Formation

The multicomponent DNAPL pool considered in this study initially consists of a mixture of 0.74 mol of PCE and 0.74 mol of 1,1,2-TCA. The initial volume of this DNAPL mixture is approximately 0.144 L. The pool is assumed to have initial length and width equal to $l_x = 0.4$ and $l_y = 0.4$ m, respectively (corresponds to $\xi = 1$), with an initial origin located at $l_{x_0} = 0.76$ m. Furthermore, the ground-water flow in the aquifer is assumed to be unidirectional with a longitudinal interstitial velocity of $U_x = 3.0 \times 10^{-3}$ m/h, whereas the ground water within the aquitard is stagnant.

The relationship between the nonaqueous-phase activity coefficients and mole fraction for a PCE and 1,1,2-TCA mixture as predicted by UNIFAC is shown in Fig. 3. For this particular two-component mixture, both of the nonaqueous-phase activity coefficients increase with decreasing mole fraction. The solubility for 1,1,2-TCA is 4.5 g/L whereas the solubility for PCE is 0.15 g/L (Mackay et al. 1992). Consequently, more 1,1,2-TCA molecules are expected to dissolve into the aqueous phase, resulting in a decreasing 1,1,2-TCA mole fraction with increasing time. Furthermore, UNIFAC estimates a higher nonaqueous-phase activity coefficient for a lower 1,1,2-TCA mole fraction (Fig. 3), which in turn leads to even faster 1,1,2-TCA depletion from the pool. The calculated mass fluxes averaged over the entire pool-water interfacial area for PCE and 1,1,2-TCA as a function of time are presented in Figs. 4(a and b), respectively. It is shown that $\bar{J}$ decreases significantly during the first 200 h after the initiation of the dissolution process. In contrast, $\hat{\bar{J}}$ decreases at a relatively slower rate. The greater the concentration gradient across the pool-water interface the greater the mass flux of the dissolved component. Therefore, the decrease of $\bar{J}$ is faster than the decrease of $\hat{\bar{J}}$ for both of the pool components because the formation of the concentration boundary layer for each dissolved component in the aquifer is relatively fast and transport is controlled by advection/dispersion whereas the contaminant transport in the aquitard is dominated by slow diffusion.

Contour plots of dissolved concentrations on the $xz$-plane along the centerline of the pool for PCE and 1,1,2-TCA at three different times are presented in Figs. 5 and 6, respectively. It should be noted that the aquifer/aquitard interface is at $z = 0$. Fig. 5 shows a gradual increase in dissolved PCE concentrations with increasing time, whereas Fig. 6 shows a decrease in dissolved 1,1,2-TCA concentrations in the vicinity of the pool from 5,000 to 10,000 h (208.3 to 416.7 days) after the initiation of the dissolution process. This concentration decrease is caused by the decreasing 1,1,2-TCA effective solubility. Because advection is the dominant transport mechanism in the aquifer whereas diffusion governs solute transport in the aquitard, dissolved contaminant molecules are expected to be transported farther downstream in the aquifer. As a result, a concentration gradient exists at the aquifer/aquitard interface

causing contaminant molecules in the aquifer to diffuse into the aquitard. Both Figs. 5 and 6 illustrate that the dissolved concentrations within the aquitard, downstream from the pool, are increasing with time.

Model simulated breakthrough concentrations for dissolved PCE and 1,1,2-TCA at a location downstream from the pool source with coordinates $x = 2.72$ m and $z = 0.024$ m are presented in Fig. 7. Both cases of an aquifer with an underlying aquitard where diffusion is included as well as an aquifer with an impermeable bedrock where diffusion is neglected are considered. It is shown that the dissolved concentrations are significantly lower in the presence of an aquitard because of contaminant diffusion into the underlying aquitard. Consequently, for certain situations back diffusion from the aquitard into the aquifer may lead to prolonged ground-water contamination. Johnson and Pankow (1992) noted that diffusion can attribute to a significant amount of contaminant storage in the aquitard, and back diffusion alone can lead to a long-lasting aquifer contamination.

Sensitivity analysis is performed to determine the impact of various ground-water velocities and aquitard retardation values on predicted downstream concentrations. A single-component PCE pool with $l_x = l_y = 0.4$ m, $l_{x_0} = 0.76$ m, and $M' = 1.415$ mol is considered. Fig. 8 shows differences between dissolved contaminant concentrations originating from identical PCE pools with and without diffusion into the aquitard. Three different ground-water velocities at three different downstream locations are examined. The percent difference in dissolved concentration is calculated by the expression: $(C^{\beta}(t) - C^{\alpha}(t)) \times 100/C^{\beta}(t)$, where $C^{\alpha}$ and $C^{\beta}$ are predicted dissolved PCE concentrations with and without diffusion into an adjacent aquitard, respectively. Fig. 9 illustrates the effect of aquitard retardation on the difference between dissolved contaminant concentrations obtained from simulations based on identical PCE pools with and without diffusion into an adjacent aquitard. Fig. 9 clearly shows that the percent difference in dissolved concentrations increases with increasing $\hat{R}$. Both Figs. 8 and 9 indicate that the highest concentration difference occurs during the initial stage of pool dissolution, and that the concentration difference decreases with time. Furthermore, Figs. 8 and 9 show the percent difference in dissolved concentrations is lowest near the pool and increases with distance away from the pool.

## Statistically Anisotropic Aquifer

Consider a single-component 1,1,2-TCA pool formed within a statistically anisotropic aquifer on top of an impermeable bedrock ($\hat{k} = 0$). The pool is assumed to have initial length and width equal to $l_x = 0.8$ and $l_y = 0.8$ m, respectively (corresponds to $\xi = 1$), with an initial origin located at $l_{x_0} = 0.68$ m. The program SPRT2D developed by Gutjahr (1989) is employed for the generation of two-dimensional realizations of statistically anisotropic, random, log-transformed hydraulic

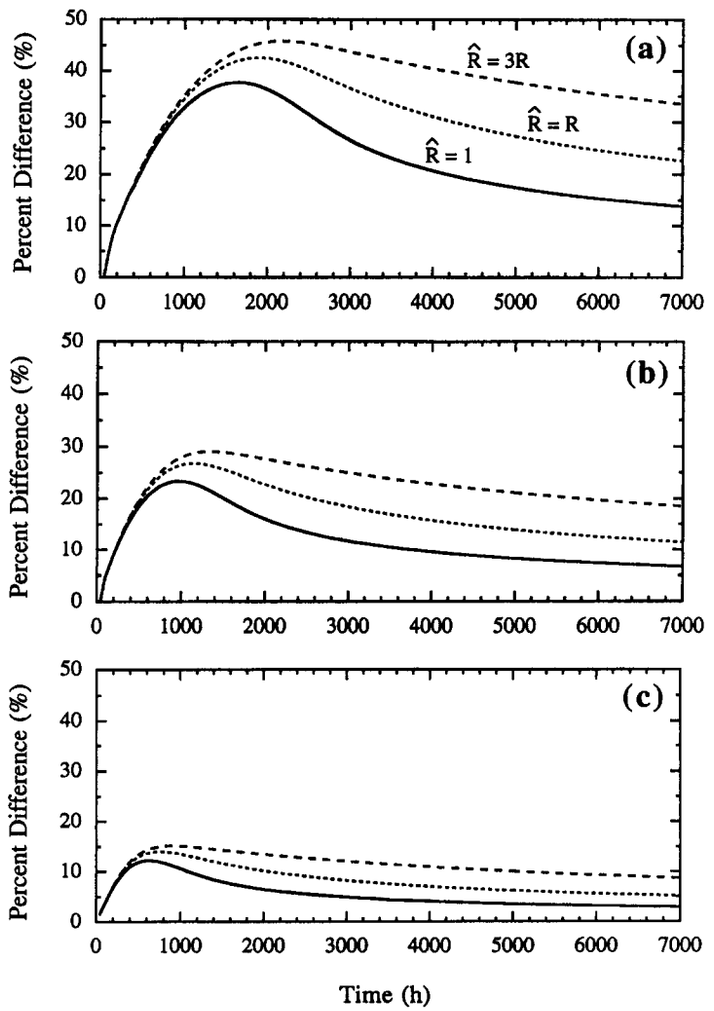


**FIG. 9. Comparison of Dissolved Concentrations Originating from Single-Component PCE Pool with and without Diffusion into Aquitard as Function of Time for Three Different Aquitard Retardation Values at Downstream Locations: (a) $x = 2.72$ m; (b) $x = 1.92$ m; (c) $x = 1.52$ m (Here $U_x = 3.0 \times 10^{-3}$ m/h; $z = 0.024$ m)**

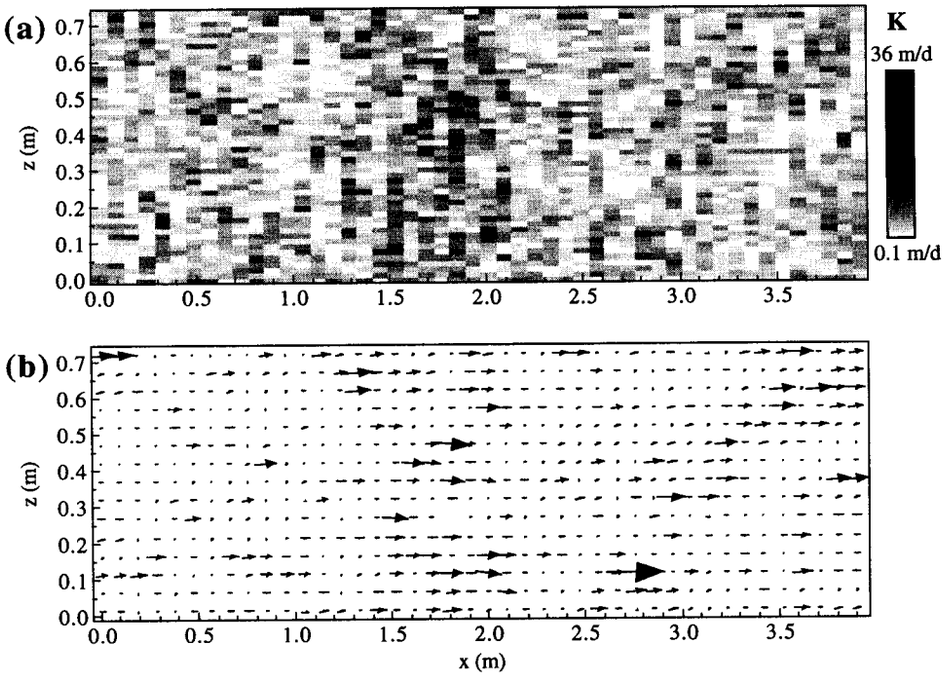


**FIG. 10. Illustration of: (a) Single Realization of Statistically Anisotropic Hydraulic Conductivity Field; (b) Corresponding Velocity Vector Field (Gray Scale Represents Magnitude of Hydraulic Conductivity, Arrow Size is Proportional to Velocity Magnitude, and Arrow Direction Indicates Flow Direction)**

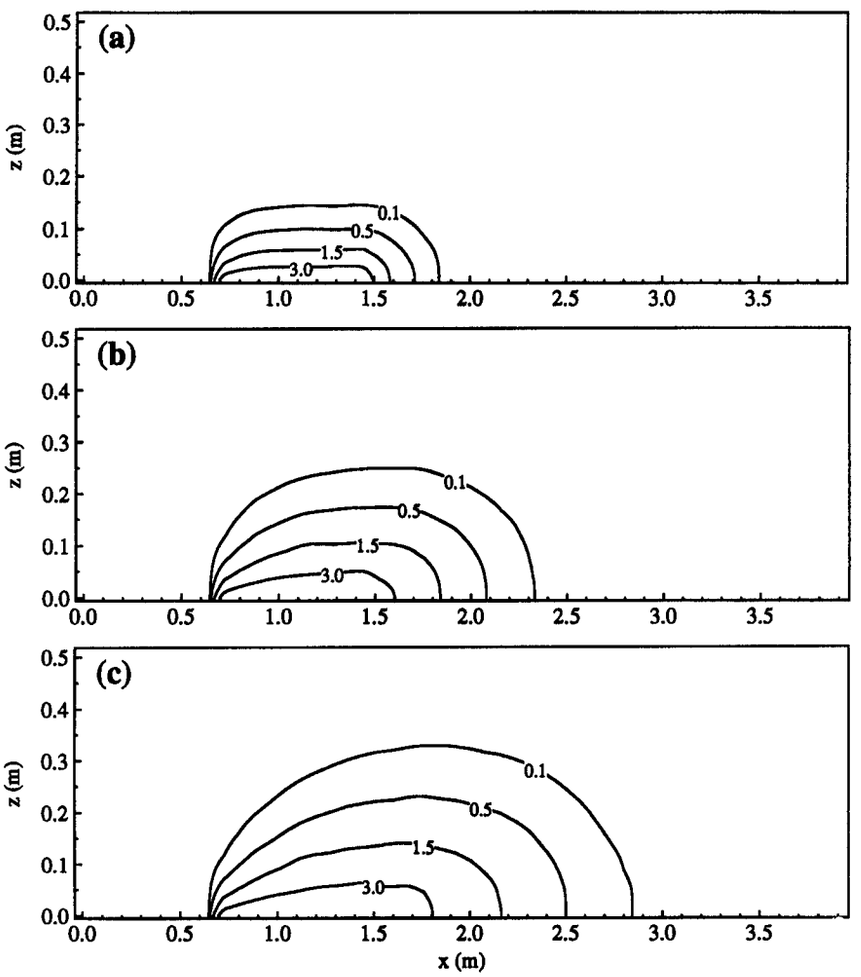


**FIG. 11. Concentration Contour Plots of 1,1,2-TCA (g/L) in Statistically Anisotropic Aquifer at: (a) 1,000; (b) 3,000; (c) 5,000 h [Since Initiation of Dissolution Process ($\sigma_Y^2 = 0.5$)]**

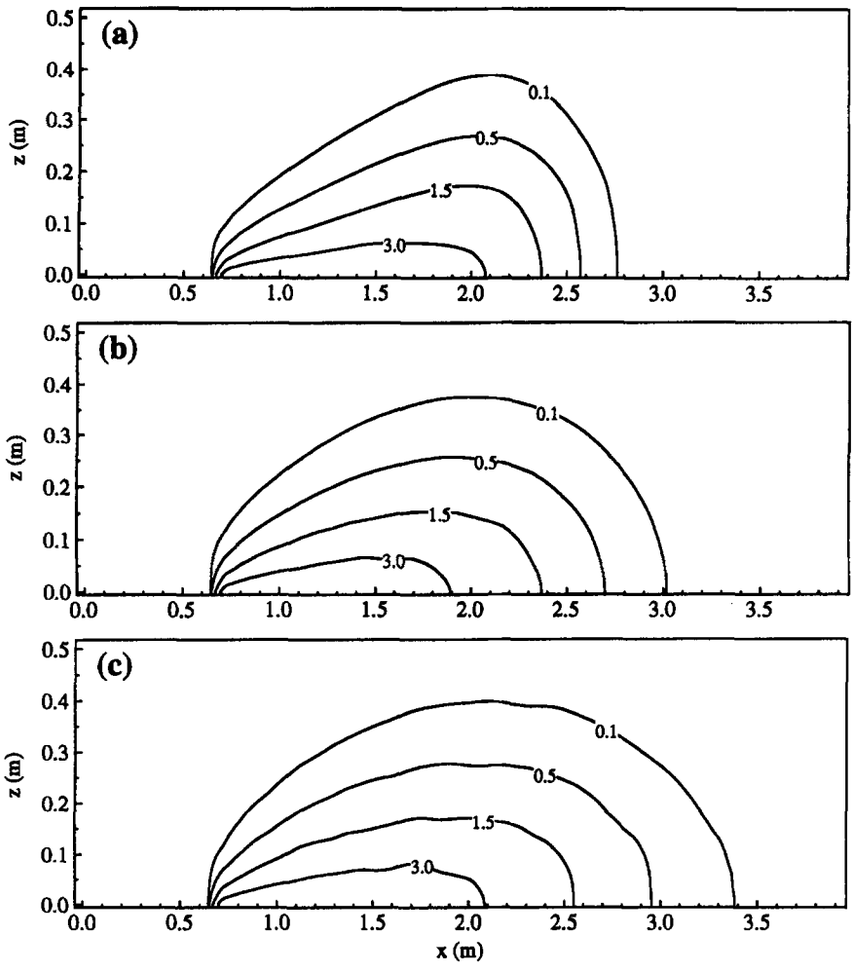


**FIG. 12. Concentration Contour Plots of 1,1,2-TCA (g/L) in Statistically Anisotropic Aquifer with: (a) $\sigma_Y^2 = 0$; (b) $\sigma_Y^2 = 0.2$; (c) $\sigma_Y^2 = 0.5$ (Here $t$ = 7,000 h)**

conductivity fields, based on the exponential covariance function (Dagan 1989). The geostatistical parameters of the $Y = \ln[K(x, z)]$ field are: $\zeta_x = 0.5$ m, $\zeta_z = 0.06$ m, $\sigma_Y^2 = 0.5$, and $\bar{Y} = 0.8$ (corresponding to a mean hydraulic conductivity $\bar{K} = 2.86$ m/day). Fig. 10(a) illustrates a single realization of the hydraulic conductivity field, where higher $K$ values are represented by darker shades and lower $K$ values are represented by lighter shades. Each rectangular unit element represents the average hydraulic conductivity at the corresponding node of the finite-difference grid used for the numerical approximations. Fig. 10(b) presents the spatially variable flow field derived from the hydraulic conductivity field of Fig. 10(a), by numerically solving (12)–(14). The flow at each node ranges from $1.15 \times 10^{-5}$ to $3.98 \times 10^{-3}$ m/h in the $x$-direction and from $-5.84 \times 10^{-4}$ to $2.22 \times 10^{-4}$ m/h in the $z$-direction, as indicated by the magnitude and direction of the arrows presented in Fig. 10(b).

The predicted 1,1,2-TCA aqueous-phase concentrations on the $xz$-plane along the centerline of the pool at three different times since the initiation of the dissolution process are presented in Fig. 11. Dissolved concentrations represent ensemble averaged obtained from 200 different realizations of the spatially variable hydraulic conductivity field. The observed result is intuitive; the plume size of the dissolved organic gradually increases in both longitudinal and vertical directions with increasing time.

The effect of the variance of the log-transformed hydraulic conductivity field $\sigma_Y^2$ on dissolved contaminant concentrations is illustrated in Fig. 12. Concentration contours are simulated with three different values of $\sigma_Y^2$ at 7,000 h (291.7 days) since the initiation of the dissolution process. With the exception of the homogeneous aquifer case [Fig. 12(a), $\sigma_Y^2 = 0$], all concentrations represent ensemble averages obtained from 200 different realizations of the spatially variable hydraulic conductivity field. Comparison of the contours presented in Fig. 12 indicates that the spreading of the dissolved organic increases with increasing $\sigma_Y^2$. However, it should be noted that the average mass flux of the 1,1,2-TCA to the aqueous phase along the pool-water interface is decreasing with increasing aquifer heterogeneity. For the conditions of Fig. 12, the calculated average mass fluxes along the pool interface are: 0.127, 0.111, and 0.107 g/h per m$^2$, for $\sigma_Y^2$ equal to 0, 0.2, and 0.5, respectively. It should be noted that for a constant $\bar{Y}$, an increase in $\sigma_Y^2$ causes an increase in $\bar{K}$, as indicated by the following relationship (Ang and Tang 1975):

$$\bar{K} = \exp\left[\bar{Y} + \frac{\sigma_Y^2}{2}\right] \tag{29}$$

The transfer of a dissolved organic into the aqueous phase is proportional to the concentration gradient at the pool interface [see (25)]. The reduction in the average mass flux $\bar{J}$ is attributed to elevated dissolved concentrations just above the pool-water interface caused by the increase in the mean hydraulic conductivity $\bar{K}$. However, it is expected that during the initial stages of the dissolution process $\bar{J}$ is directly proportional to $\sigma_Y^2$ because the concentration gradients along the pool-water interface are large at early time. Therefore, for constant saturation concentration along the pool-water interface and steady-state flow conditions, the transfer of the dissolved 1,1,2-TCA

is slower and the spreading of the plume is greater within statistically anisotropic aquifers than within homogeneous aquifers.

## SUMMARY

A two-dimensional finite-difference numerical model simulating solute transport resulting from the dissolution of single- and multicomponent NAPL pools in heterogeneous subsurface formations is presented. Multicomponent dissolution is modeled using an effective solubility relationship, where the nonaqueous-phase activity coefficient for each constituent is evaluated at each and every time step. Subsurface heterogeneities are depicted by an ideally stratified porous medium and by a statistically anisotropic aquifer. For solute transport in a stratified porous medium consisting of a sand aquifer over a clay aquitard, model simulations indicate that lower solute concentrations in the aquifer are expected when diffusion into the aquitard is considered. Consequently, back diffusion from the clay aquitard into the aquifer may lead to prolonged ground-water contamination. For solute transport in a statistically anisotropic aquifer, it was shown that for the case of constant saturation concentration along the NAPL pool-water interface and steady-state flow conditions, the predicted average mass flux is lower, but the spreading of dissolved contaminants is greater in statistically anisotropic than homogeneous water-saturated subsurface formations.

## ACKNOWLEDGMENTS

This research was sponsored by the Environmental Protection Agency, under grant no. R-823579-01-0. However, the manuscript has not been subjected to the agency's peer and administrative review and therefore does not necessarily reflect the views of the agency, and no official endorsement should be inferred. Kenneth Y. Lee is grateful for the additional support provided by a fellowship from the Fluor Daniel Corporation. The writers thank Susan Powers for her helpful suggestions.

## APPENDIX I. REFERENCES

Anderson, M. R., Johnson, R. L., and Pankow, J. F. (1992). "Dissolution of dense chlorinated solvents into groundwater, 3, modeling contaminant plumes from fingers and pools of solvent." *Envir. Sci. and Technol.*, 26(5), 901–908.

Ang, A. H.-S., and Tang, W. H. (1975). *Probability concepts in engineering planning and design, volume I—basic principles*. Wiley, New York, N.Y.

Ball, W. P., and Roberts, P. V. (1991). "Long-term sorption of halogenated organic chemicals by aquifer material, 1, equilibrium." *Envir. Sci. and Technol.*, 25(7), 1223–1237.

Banerjee, S. (1984). "Solubility of organic mixtures in water." *Envir. Sci. and Technol.*, 18(8), 587–591.

Bear, J. (1979). *Hydraulics of groundwater*. McGraw-Hill, Inc., New York, N.Y.

BRI. (1993). *PC-UNIFAC-4.0*. BRI, Atlanta, Ga.

Broholm, K., and Feenstra, S. (1995). "Laboratory measurements of the aqueous solubility of mixtures of chlorinated solvents." *Envir. Toxicol. and Chem.*, 14, 9–15.

Burr, D. T., Sudicky, E. A., and Naff, R. L. (1994). "Nonreactive and reactive solute transport in three-dimensional heterogeneous porous media: Mean displacement, plume spreading, and uncertainty." *Water Resour. Res.*, 30(3), 791–815.

Chrysikopoulos, C. V. (1995). "Three-dimensional analytical models of contaminant transport from nonaqueous phase liquid pool dissolution in saturated subsurface formations." *Water Resour. Res.*, 31(4), 1137–1145.

Chrysikopoulos, C. V., and Lee, K. Y. (1998). "Contaminant transport resulting from multicomponent nonaqueous phase liquid pool dissolution in three-dimensional subsurface formations." *J. Contaminant Hydr.*, 31(1-2), 1–21.

Chrysikopoulos, C. V., Voudrias, E. A., and Fyrillas, M. M. (1994). "Modeling of contaminant transport resulting from dissolution of nonaqueous phase liquid pools in saturated porous media." *Transp. in Porous Media*, 16(2), 125–145.

Dagan, G. (1989). *Flow and transport in porous formations*. Springer-Verlag, New York, N.Y.

de Marsily, G. (1986). *Quantitative hydrogeology, groundwater hydrology for engineers*. Academic Press, San Diego, Calif.

Fredenslund, A., Gmehling, J., and Rasmussen, P. (1977). *Vapor-liquid equilibria using UNIFAC*. Elsevier, New York, N.Y.

Freeze, R. A. (1975). "A stochastic-conceptual analysis of one-dimensional groundwater flow in nonuniform homogeneous media." *Water Resour. Res.*, 11(5), 725–741.

Gelhar, L. W. (1993). *Stochastic subsurface hydrology*. Prentice-Hall, Inc., Englewood Cliffs, N.J.

Gelhar, L. W., and Axness, C. L. (1983). "Three-dimensional stochastic analysis of macrodispersion in aquifers." *Water Resour. Res.*, 19(1), 161–180.

Gutjahr, A. L. (1989). "Fast Fourier transform for random field generation." *Proj. Rep. Contract No. 4-R58-2690R*, for Los Alamos Grant, New Mexico Institute of Mining and Technology, Socorro, N.M.

Hashimoto, I., Deshpande, K. B., and Thomas, H. C. (1964). "Peclet numbers and retardation factors for ion exchange columns." *Industrial and Engrg. Chem. Fundamentals*, 3(3), 213–218.

Hayduk, W., and Laudie, H. (1974). "Prediction of diffusion coefficients for nonelectrolytes in dilute aqueous solutions." *AIChE J.*, 20(3), 611–615.

Holman, H.-Y. N., and Javandel, I. (1996). "Evaluation of transient dissolution of slightly water-soluble compounds from a light nonaqueous phase liquid pool." *Water Resour. Res.*, 32(4), 915–923. [Correction (1996). *Water Resources Research*, 32, 1917.]

Incropera, F. P., and DeWitt, D. P. (1990). *Fundamentals of heat and mass transfer*, 3rd Ed., Wiley, New York, N.Y.

Johnson, R. L., and Pankow, J. F. (1992). "Dissolution of dense chlorinated solvents into groundwater, 2, source functions for pools of solvent." *Envir. Sci. and Technol.*, 26(5), 896–901.

Karickhoff, S. W. (1984). "Organic pollutant sorption in aquatic systems." *J. Hydr. Engrg.*, ASCE, 110(6), 707–735.

Lee, K. Y., and Chrysikopoulos, C. V. (1995). "Numerical modeling of three-dimensional contaminant migration from dissolution of multicomponent NAPL pools in saturated porous media." *Envir. Geol.*, 26(3), 157–165.

Lyman, W. J., Reehl, W. F., and Rosenblatt, D. H. (1982). *Handbook of chemical property estimation methods*. McGraw-Hill, Inc., New York, N.Y.

Mackay, D., Shiu, W. Y., and Ma, K. C. (1992). *Illustrated handbook of physical-chemical properties and environmental fate for organic chemicals, Vol. 3, volatile organic chemicals*. Lewis Publishers, Chelsea, Mich.

Mackay, D. M., Roberts, P. V., and Cherry, J. A. (1985). "Transport of organic contaminants in groundwater." *Envir. Sci. and Technol.*, 19(5), 384–392.

Manivannan, I., Powers, S. E., and Curry, G. W. Jr. (1996). "Dissolution of NAPLs entrapped in heterogeneous porous media." *Non-aqueous phase liquids (NAPLs) in subsurface environment: Assessment and remediation*, L. N. Reddi, ed., American Society of Civil Engineers, New York, N.Y., 563–574.

Mason, A. R., and Kueper, B. H. (1996). "Numerical simulation of surfactant-enhanced solubilization of pooled DNAPL." *Envir. Sci. and Technol.*, 30, 3205–3215.

Mercer, J. W., Skipp, D. C., Giffin, D., and Ross, R. R. (1990). "Basics of pump-and-treat groundwater remediation technology." *Rep. No. EPA-600/8-90/003*, Robert S. Kerr Environmental Research Laboratory, Ada, Okla.

Myrand, D., Gillham, R. W., Sudicky, E. A., O'Hannesin, S. F., and Johnson, R. L. (1992). "Diffusion of volatile organic compounds in natural clay deposits: Laboratory tests." *J. Contaminant Hydro.*, 10(2), 159–177.

Russo, D., Zaidel, J., and Laufer, A. (1994). "Stochastic analysis of solute transport in partially saturated heterogeneous soil, 1, numerical experiments." *Water Resour. Res.*, 30(3), 769–779.

Schwarzenbach, R. P., Gschwend, P. M., and Imboden, D. M. (1993). *Environmental organic chemistry*. Wiley, New York, N.Y.

Seagren, E. A., Rittman, B. E., and Valocchi, A. J. (1994). "Quantitative evaluation of the enhancement of NAPL-pool dissolution by flushing and biodegradation." *Envir. Sci. and Technol.*, 28, 833–839.

Stumm, W., and Morgan, J. J. (1981). *Aquatic chemistry*, 2nd Ed., Wiley, New York, N.Y.

Sudicky, E. A. (1986). "A natural gradient experiment on solute transport in a sand aquifer: Spatial variability of hydraulic conductivity and its role in the dispersion process." *Water Resour. Res.*, 22(13), 2069–2082.

Voudrias, E. A., and Yeh, M. F. (1994). "Dissolution of a toluene pool

under constant and variable hydraulic gradients with implications for aquifer remediation." *Groundwater*, 32(2), 305–311.
Whelan, M. P., Voudrias, E. A., and Pearce, A. (1994). "DNAPL pool dissolution in saturated porous media: Procedure development and preliminary results." *J. Contaminant Hydrol.*, 15(3), 223–237.

## APPENDIX II. NOTATION

*The following symbols are used in this paper:*

$A$ = pool-water interfacial area ($L^2$);
$C$ = aqueous-phase solute concentration (solute mass per fluid volume) ($M\ L^{-3}$);
$C_b$ = background aqueous-phase solute concentration (solute mass per fluid volume) ($M\ L^{-3}$);
$C_s$ = single-component aqueous saturation concentration (solubility) ($M\ L^{-3}$);
$C^w$ = effective solubility ($M\ L^{-3}$);
$\mathcal{D}$ = molecular diffusion coefficient ($L^2\ T^{-1}$);
$\mathcal{D}_e$ = effective molecular diffusion coefficient: $\mathcal{D}/\tau^*$ ($L^2\ T^{-1}$);
$D_x$ = longitudinal hydrodynamic dispersion coefficient ($L^2\ T^{-1}$);
$D_z$ = hydrodynamic dispersion coefficient in vertical direction ($L^2\ T^{-1}$);
$d$ = pool thickness (L);
$f_{oc}$ = organic carbon fraction (mass of organic carbon per mass of sorbent) ($M\ M^{-1}$);
$h$ = total head potential (L);
$I(\ )$ = integer mode arithmetic operator;
$J$ = local mass flux ($M\ L^{-2}\ T^{-1}$);
$\bar{J}$ = average (or overall) mass flux ($M\ L^{-2}\ T^{-1}$);
$K$ = hydraulic conductivity ($L\ T^{-1}$);
$\bar{K}$ = mean hydraulic conductivity ($L\ T^{-1}$);
$K_d$ = distribution coefficient ($L^3\ M^{-1}$);
$K_{oc}$ = organic carbon partition coefficient (mass sorbed per unit mass of organic carbon per unit aqueous concentration) ($L^3\ M^{-1}$);
$k$ = local mass transfer coefficient ($L\ T^{-1}$);
$\bar{k}$ = average (or overall) mass transfer coefficient ($L\ T^{-1}$);
$l_x$ = length of pool in longitudinal direction (L);
$l_{x_0}$ = $x$ Cartesian coordinate of pool origin (L);
$l_y$ = width of pool in lateral direction (L);
$\mathcal{M}$ = number of moles in NAPL pool mixture;
$\mathcal{M}'$ = initial number of moles in NAPL pool mixture;
$m$ = integer time step summation index;
$m_f$ = total number of time steps;
$\mathcal{P}$ = total number of components;
$p$ = component number indicator (subscript);
$R$ = retardation factor;
$r$ = separation distance of hydraulic conductivity measurements (L);
$t$ = time (T);
$U_x$ = ground-water velocity in longitudinal direction ($L\ T^{-1}$);
$U_z$ = ground-water velocity in vertical direction ($L\ T^{-1}$);
$\mathbf{U}$ = interstitial velocity vector;
$V$ = molar volume ($L^3\ mol^{-1}$);
$X$ = nonaqueous-phase mole fraction;
$x$ = spatial Cartesian coordinates in longitudinal direction (L);
$Y$ = log-transformed hydraulic conductivity, equal to ln $K$;
$\bar{Y}$ = mean log-transformed hydraulic conductivity;
$z$ = spatial Cartesian coordinates in vertical direction (L);
$\alpha_L$ = longitudinal dispersivity (L);
$\alpha_T$ = transverse dispersivity (L);
$\gamma$ = nonaqueous-phase activity coefficient;
$\Delta t$ = numerical time step (T);
$\zeta$ = correlation length scale (L);
$\eta_w$ = water viscosity ($M\ L^{-1}\ T^{-1}$);
$\theta$ = effective porosity (fluid volume per porous medium volume) ($L^3\ L^{-3}$);
$\lambda$ = first-order decay constant ($T^{-1}$);
$\xi$ = ratio of pool length to pool width;
$\rho_b$ = bulk density of porous medium ($M\ L^{-3}$);
$\rho_p$ = density of NAPL component $p$ ($M\ L^{-3}$);
$\sigma_Y^2$ = variance of ln $K$;
$\tau^*$ = tortuosity; and
$\hat{\ }$ = parameters associated with aquitard are indicated by "hat."